JOURNAL OF MATERIALS SCIENCE 28 (1993) 5079–5087

Solid-state bonding of single-crystals of $Ni_{(111)}/Al_2O_{3(0001)}$

C. WAN, M. DUPEUX
Laboratoire de Thermodynamique et Physico-Chimie Métallurgiques (UA 29 CNRS), ENSEEG, Institut National Polytechnique de Grenoble, Domaine Universitaire, BP 75, 38402 Saint Martin d'Hères cedex, France

Some fundamental aspects of the solid state bonding process between single crystals of alumina and nickel were studied. It was shown that a model formerly developed to account for the kinetics of diffusion bonding between two metals can be adapted to the case of a metal–ceramic couple. A coincidence site lattice calculation proved that one of the crystallographic relative orientations often mentioned in literature was certainly energetically favourable. With this relative orientation, several nickel–alumina bicrystals have been produced by solid state bonding under secondary vacuum. The influence of operating conditions such as contact pressure and annealing duration has been explored and compared with the calculated results of the bonding kinetics model. Characterization of the solid-state bonded interface was undertaken by optical microscopy and scanning as well as transmission electron microscopy. Observations prove that the initial imposed crystallographic relative orientation was maintained during the solid-state bonding process, and that the synthetic alumina–nickel interface obtained by this technique was free from reaction layer at the usual TEM scale.

1. Introduction

Ni/Al_2O_3 interfaces are considered here as a model system for metal–ceramic joints. These may be encountered mainly in composite materials designed for high-temperature applications and in structural metal–ceramic junctions.

Solid-state bonded Ni/Al_2O_3 joints have been produced or mentioned by several groups [1–12] who suggested that the junctions should be made under an inert atmosphere or under a high vacuum. Calow *et al.* [4, 5] indicated that the junctions obtained under high vacuum had the highest strength.

However, joining of Al_2O_3/Ni single crystals on both sides has not been found so far in the literature, except for the epitaxial $Ni_{(1\,1\,1)}/Al_2O_{3(0\,0\,0\,1)}$ interface obtained by the vapo-deposition of nickel on a (0 0 0 1) plane of Al_2O_3 reported by Drillet [1]. Because of the strong dependence of the phase-boundary energy on the relative orientations of the adjacent crystals, there is a fundamental interest in the possibility of making such orientation-controlled bicrystals in order to study the influence of the crystallographic relative orientation on the chemistry, atomic scale structure and eventually mechanical strength of the metal–ceramic interface.

Several theoretical models have been proposed concerning the mechanisms of joining metals to ceramics, and especially nickel to Al_2O_3. The most common among these are the model of cavity diffusion and evaporation–condensation in the interface [2, 3], and the model involving chemical interfacial reactions. In the second case, it was considered that the formation of an intermediate phase of the spinel type ($NiAl_2O_4$) plays an important role [4, 5, 11]. However, Al_2O_3/Ni junctions have also been achieved without detecting the formation of spinel at the interface [12]. Finally, the question is far from being clear as to what role the spinel might play in the junction mechanism. This was also one of our reasons for studying the solid-state bonding of single crystals of nickel and alumina.

2. Preliminary calculations

2.1. Choice of crystallographic relative orientations

The modelling of grain-boundary structure has been undertaken by various ways in the literature. In the first one, the positions of each atom neighbouring the joint is calculated according to an interatomic potential model, based on a minimal free-energy criterion [13, 14]. In a second approach, which we have used, only geometrical conditions are considered to determine the common sites of two interpenetrating crystal lattices. From here onwards, the concept of the coincidence site lattice (CSL) has been developed.

A decisive contribution was made by the 0-lattice theory of Bollmann [15–17]. For all possible relative orientations of two identical lattices that are imagined to be interpenetrated, the 0-points are the sites where the two crystal lattices, 1 and 2, show the best fit, and correspond to minimal strain points (MS-points). Assuming **A** to be a linear transformation matrix which transforms points of lattice 1 into points of lattice 2, Bollmann showed that if $\boldsymbol{b}^L$ is a translation vector of crystal lattice 1, the coordinates $\boldsymbol{x}^0$ of possible geo-

0022–2461

metric coincidence points (0-points) are given by:

$$(\mathbf{I} - \mathbf{A}^{-1})x^0 = b^L \quad (1)$$

where $\mathbf{I}$ is the matrix of the unit transformation. The 0-points which are solutions of this equation define a coincidence site lattice common to both crystals, the unit cell of which has an integer multiple volume of each unit cell of the basic lattices. The integer order of multiplicity Σ of this unit cell is then called the coincidence index.

The 0-lattice with its unit cell introduces a periodic structure in the interpenetrated crystal lattices. A position and an orientation can be fixed for a grain boundary. Then the atoms of one side of the boundary will take the position of crystal 1 and those of the other side, those of crystal 2. The structure of the boundary itself is the consequence of the 0-lattice structure. An optimum stable boundary is basically characterized by a minimal boundary free energy. It is generally considered that the boundary for which the primitive unit cell of the 0-lattice is the nearest possible to that of the crystal lattices (that is for which Σ is the smallest) has the lowest energy. In addition, the energy can be further minimized if the boundary plane has such an orientation that it could pass through the greatest possible number of sites of the 0-lattice. Both arguments are based on the implicit consideration that when the surface density of good fit sites is high in the boundary, the strain-energy term in the total energy of the boundary is low. This criterion may be taken as reasonably confirmed by experimental observations, rather than as theoretically supported [14].

An extension of the CSL theory from the case of grain boundaries to that of phase boundaries has been proposed by Bonnet and Durand [18]. The fundamental difference in that second case is that there can no longer exist any exact coincidence between the two lattices. An additional small deformation is therefore necessary to transform a near coincident multiple cell of the lattice 1, with index Σ_1, to another near coincident cell of the lattice 2, with index Σ_2. A computer calculation technique was developed by Bonnet to determine the pairs of multiple cells of the crystal lattices 1 and 2 which can be closely superimposed for all possible relative orientations of two crystal lattices. The program indicates the orientations of the crystal lattice 2 with respect to lattice 1 for which a near coincident multiple cell can be found up to a limiting value of the coincidence indices, calculates the corresponding indices Σ_1 and Σ_2 as well as the tensor of the necessary deformation to transform one into another [19].

Although a program calculating three-dimensional coincidence was available, the computation time is considerably long. In addition, the results of such a calculation almost always give at least a dense plane of crystal 1 parallel to another dense plane of crystal 2, and the favourable orientation of the phase boundary parallel to these two planes [20]. Therefore, it is reasonable to investigate only the two-dimensional coincidence possibilities, with a set of imposed coincidence planes (chosen from the densest planes of the two crystal lattices) and exploring only the relative rotations, plane on plane, of two two-dimensional unit cells defined in each of them to look for the best fitting of these two planes.

It is logical to choose the imposed coincidence planes based on the spontaneous relative orientations already observed experimentally. From the point of view of the geometric coincidence between α-alumina lattice and cubic metals, Mulder and Klomp [21] proposed that the three-fold symmetry planes $\{1\,1\,1\}$ of the metals should be more easily fitted to the hexagonal planes $(0\,0\,0\,1)$ of sapphire. From the point of view of the gain of surface energy during the formation of the interface, they suggested, however, that the $\{1\,1\,0\}$ planes of the metals were more favourable than the $\{1\,1\,1\}$ planes for joining to $(0\,0\,0\,1)$ planes of sapphire. Following these considerations, together with experimental observations, Fischmeister *et al.* [22] concluded that the relative orientations presented in Table I should give the strongest interface, with rather small Σ indices and strains. In addition, let us recall the results of Drillet [1] showing from vapour-deposition experiments that the interface with $(1\,1\,1)_{Ni} \| (0\,0\,0\,1)_{Al_2O_3}$ seems more stable.

Thus we chose the $(0\,0\,0\,1)$ and $(1\,1\,\bar{2}\,0)$ planes of alumina and the $(1\,1\,1)$, $(1\,1\,0)$ and $(1\,0\,0)$ planes of nickel as common dense planes for the calculation of two-dimensional coincidence with help of a FORTRAN program due to Bonnet and already used in a previous work [23]. The basic vectors of the planar unit cells used in the calculation are presented in Table II. They are based on the hexagonal and rhombohedral descriptions of the α-Al_2O_3 crystal [24], and on the rhombohedral unit cell of the f c c nickel crystal. The calculated results which are presented in Table III show that the indices Σ_1 and Σ_2 of the couple of planes $(0\,0\,0\,1)_{Al_2O_3}/(1\,1\,1)_{Ni}$ with a relative rotation of zero degree of the chosen planar unit cells, are the smallest among those calculated, with a reasonable value of the sum of absolute values of the principal strains. Thus, the computed CSL results are in agreement with the conclusions of the previous works mentioned above, especially with Drillet's observations. For instance, Drillet also observed the relative orientations with $(0\,0\,0\,1)_{Al_2O_3} \| (1\,0\,0)_{Ni}$, $[\bar{1}\,2\,\bar{1}\,0]_{Al_2O_3} \| [0\,1\,1]_{Ni}$ (equivalent to the fifth line of our Table III) in polycrystalline Ni/Al_2O_3 thin foils after solid-state bonding. So, similar to cases previously mentioned in literature [14], this is again an example in which the observed orientation relationships satisfy the low Σ criterion, but other low Σ relative orientations found from the CSL calculation

TABLE I Low-energy relative orientations between cubic metals and sapphire, after Fischmeister *et al.* [22]

$(1\,1\,0)_{Nb} \| (0\,0\,0\,1)_{Al_2O_3}$,	$[0\,0\,1]_{Nb} \| [2\,\bar{1}\,\bar{1}\,0]_{Al_2O_3}$
$(1\,1\,0)_{Nb} \| (0\,0\,0\,1)_{Al_2O_3}$,	$[0\,0\,1]_{Nb} \| [0\,1\,\bar{1}\,0]_{Al_2O_3}$
$(1\,1\,0)_{Nb} \| (2\,\bar{1}\,\bar{1}\,0)_{Al_2O_3}$,	$[0\,0\,1]_{Nb} \| [0\,0\,0\,1]_{Al_2O_3}$
$(1\,1\,0)_{Nb} \| (2\,\bar{1}\,\bar{1}\,0)_{Al_2O_3}$,	$[0\,0\,1]_{Nb} \| [0\,1\,\bar{1}\,0]_{Al_2O_3}$
$(1\,1\,1)_{Pd} \| (0\,0\,0\,1)_{Al_2O_3}$,	$[1\,1\,0]_{Pd} \| [0\,1\,\bar{1}\,0]_{Al_2O_3}$

TABLE II Basic vectors of the planar unit cells used for calculations of the two-dimensional coincidence orientations (x and y are the calculation axes)

Crystal planes	Basic vector in coordinates	Component (nm) *a*	Component (nm) *b*
$(0001)_{Al_2O_3}$	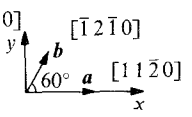	0.4759 0	0.2380 0.4121
$(11\bar{2}0)_{Al_2O_3}$	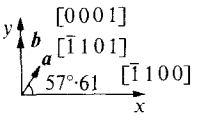	0.2747 0.4330	0 1.2991
$(111)_{Ni}$	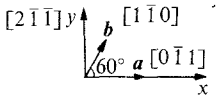	0.2492 0	0.1246 0.2156
$(110)_{Ni}$	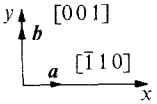	0.2492 0	0 0.3524
$(100)_{Ni}$	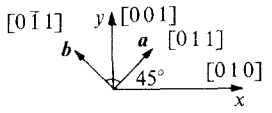	0.1762 0.1762	−0.1762 0.1762

TABLE III Calculated results of planar coincidence

Common planes		Rotation (deg)	Σ_1 (minimum)	Σ_2 (minimum)	$\varepsilon = \lvert\varepsilon_1\rvert + \lvert\varepsilon_2\rvert + \lvert\varepsilon_3\rvert$
1, Al_2O_3	2, Ni				
0001	111	0	1	4	0.09007
0001	110	0	5	12	0.07037
0001	110	35.3	5	12	0.07037
0001	110	60.0	5	12	0.07037
0001	100	15.0	3	10	0.05260
11$\bar{2}$0	111	32.3	2	14	0.08768
11$\bar{2}$0	110	59.9	2	8	0.09066
11$\bar{2}$0	100	27.5	2	11	0.05648

have not been actually observed (for instance $(11\bar{2}0)_{Al_2O_3} \parallel (110)_{Ni}$, 59.9°).

In conclusion, the schematic interface on Fig. 1 seems likely to produce the best junctions between single crystals of alumina and nickel. Therefore, this is the crystallography chosen for the specimens prepared in the present work.

2.2. Solid-state bonding kinetics

Garmong *et al.* [25] proposed a model based on a previous work by Hamilton [26] to described the achievement of full interfacial contact between two metals which are joined by diffusion bonding in the solid state. We attempted to apply this model to our case (solid-state bonded joints between a metal, nickel, and a ceramic, Al_2O_3) with the only additional hypothesis of the absence of plastic deformation of the alumina during the thermocompression. This hypothesis appears to be reasonable, considering the difference in mechanical properties of the two materials involved at the bonding temperature.

As in the case of two metals, the experimental works quoted earlier in this paper underlined that the best solid-state bonded junctions between a metal and a ceramic can only be achieved with a perfect interfacial contact, up to a point when the interface porosities are thoroughly eliminated. It can be considered, as assumed by Garmong *et al.* [25], that the surfaces to be welded possess a bimodal distribution of asperities, i.e. small asperities of short wavelength superimposed on long wavelength asperities, all caused by the polishing or processing carried out during the surface preparations.

For a well-polished laboratory platelet of ceramic or metal it can be considered that the long wavelength asperities are negligible, or rather coincide with the average profile of the specimen itself. That is, only the

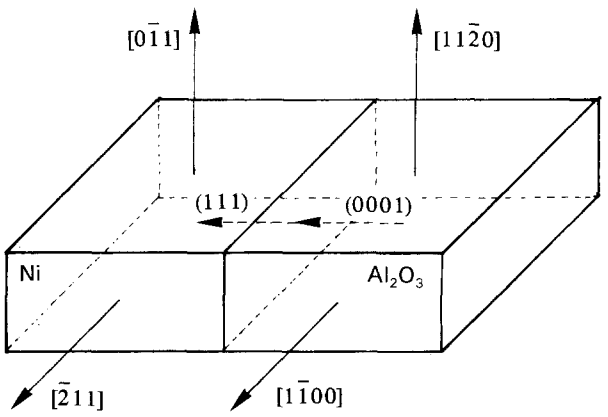

Figure 1 Schematic drawing of the relative orientations chosen in the present work.

short wavelength asperities are present, and distributed on a nearly perfectly flat surface. Indeed, the surface roughness measurement we carried out on our alumina single-crystal platelets showed an average roughness $R_a \leqslant 10$ nm on a circular surface presenting a convex curvature of the order of 0.2 μm for a diameter of 10 mm (i.e. a 2×10^{-5} planarity defect). Similarly, measurements on our nickel single-crystal platelets after polishing indicated an average roughness less than 0.5 μm. The asperities on the ceramic and those on the metal must be eliminated either by flattening or by filling of cavities, so that the surfaces to be welded can be in contact at the atomic scale along the entire surface for the junction to be optimal.

According to Garmong *et al.* [25], two mechanisms are involved in the development of the full physical contact. At first, the plastic deformation of the metal under the applied contact pressure helps to reduce the height of the asperities and the size of cavities left between them. Second, the remaining porosities can be eliminated by the vacancy diffusion under a thermodynamic force driven by the pore surface energy and by the applied stress. This second mechanism is similar to the final stage of the sintering of powder compacts.

The procedure of development of the full physical contact along the interface can therefore be divided into two stages. The first mechanism alone, namely creep of long wavelength asperities, acts during the first stage. As long as the size of the residual cavities is still relatively large, the contribution of the vacancy diffusion may be neglected. The first stage reaches its end when the asperities of long wavelength are smoothed down to the level of the top of asperities of short wavelength. During the second stage, both mechanisms (plasticity and vacancy diffusion) can be jointly efficient to annihilate the remaining porosities which are of small size.

To model the first stage, Garmong *et al.* [25] divided each asperity of long wavelength into thin slices of width w parallel to the base of the asperity of width w_b and perpendicular to the average applied pressure, P_{ext}, during the bonding process. A creep constitutive equation of the material is needed and taken under the form

$$\dot{\varepsilon} = K_1(\sigma - \sigma_0) + K_2\sigma^n \quad (2)$$

where $\dot{\varepsilon}$ is the creep rate, σ the applied stress, taken equal to the uniaxial bonding pressure P_{ext}, K_1, K_2, σ_0 and n are constants determined from experiments. During Stage I, Garmong *et al.* [25] showed that the dimensionless parameter $u = w/w_b$ for each slice must fulfil the following differential equation

$$\frac{du}{dt} = \frac{3^{1/2}}{2}\left[K_1\left(\frac{3^{1/2}}{2}P_{ext} - u\sigma_0\right) + K_2 u\left(\frac{3^{1/2}P_{ext}}{2\ u}\right)^n\right] \quad (3)$$

The resolution of this equation gives a dimensionless width for each slice at every instant. Considering the conservation of the volume of every slice during the plastic deformation and the initial shape of the asperity, the width and thickness of each slice can be deduced, from which the shape change of the asperity and the instant depth of the long wavelength porosity left at time t. When the short wavelength asperities on either side of the interface start to come into contact, Stage I is accomplished and Stage II begins.

To model this second stage, Garmong *et al.* [25] proposed that the radius, a, of the residual porosity fulfils this second differential equation

$$\frac{da}{dt} = -\left\{\left[\frac{D_v\Omega 1}{kT\ a}\left(\frac{2\gamma}{a} + P_{ext}\right)\right] + \frac{3}{4}K_1 a\left(2\sigma_0 \ln\frac{b}{a} + \frac{2\gamma}{a} + P_{ext}\right)\right\} \quad (4)$$

where D_v and Ω are, respectively, the diffusion coefficient and the volume of a lattice vacancy, k is Boltzmann's constant, T the absolute temperature, γ the pore surface energy, b half the distance between two neighbouring pores, t the time, K_1 and σ_0 are constants in the constitutive creep law of the form

$$\dot{\varepsilon} = K_1(\sigma - \sigma_0) \quad (5)$$

Two FORTRAN programs written by Dupeux and co-workers for the numerical resolution of Equations 3 and 4 were available. They had allowed previous successful applications of the model to the bimetallic systems Al/Al_2Cu, Ag/Cu [27] and Ni/Ni_3Al [28]. Using these two programs, in addition to our hypothesis mentioned above (undeformability of the alumina), we could apply this model to the system Ni/Al_2O_3.

The values of constants taken for our calculations are presented in Table IV. A few preliminary results calculated to help the choice of our experimental parameters are shown in Table V. The initial value of short wavelength porosity size $a = 1$ μm has been chosen to integrate Equation 4. This value is indeed certainly an overestimation of the real one, as we have seen from the average roughness measurements mentioned. However, even with this initial value, the duration of Stage II always appears markedly shorter than that of Stage I.

TABLE IV Data used for the calculations of diffusion-bonding kinetics

Constant	Value	References
K_1	0	[29]
K_2	7.79×10^{-7} (N mm^{-2})$^{-n}$ h^{-1}	[29]
n	4.6	[29]
σ_0	0	[29]
D_v	1.07×10^{-5} mm^2 h^{-1}	[29]
Ω	10.72×10^{-21} mm^3	[29]
T	1373 K	[29]
k	1.38×10^{-20} mJ K^{-1}	[29]
γ	1810 mJ m^{-2}	[30]

TABLE V Time for complete closure of interfacial cavities with 1 μm initial diameter in Al_2O_3/Ni at 1100 °C, calculated according to the model of Garmong *et al.* [25]

P_{ext} (MPa)	Duration (h)		Total time (h)
	Stage I	Stage II	
5	> 160	8	> 160
6	160	8	168
7	80	7	87
8	50	6	56
9	30	6	36
10	20	6	26

3. Experimental procedure

α-Al_2O_3 cylindrical platelets were provided by Criceram (France), of 10 ± 0.1 mm diameter, and thickness 3 ± 0.2 mm. One of the faces was cut and polished parallel to the crystallographic plane (0 0 0 1). Before use, α-Al_2O_3 specimens were ultrasonically cleaned in acetone and then annealed at 1100 °C under 10^{-5} mbar for 1 h.

The nickel single crystal we used was produced by the Ecole Nationale Superieure des Mines de Saint-Etienne (France). Its nominal purity was 99.95 wt %. The oxygen content was verified to be less than 49 at. p.p.m. The specimen was cut into slices of the desired size, about $3 \times 10 \times 10$ mm^3, by spark machining. The crystallographic orientation was chosen and controlled by X-ray back-scattered Läue patterns. The face to be welded was cut parallel to the (1 1 1) plane. This face was polished with diamond paste down to 1 μm, and then ultrasonically cleaned in acetone.

The bonding treatments were performed in a compression creep device adapted to high vacuum (10^{-5} mbar) [31]. This machine has an electric furnace with a 1100 °C maximum practical temperature. With molybdenum interpenetrating compression jaws, a uniaxial contact pressure can be applied to the two slices of specimens (nickel and Al_2O_3) suitably superimposed according to the orientation relationships chosen from the previous calculation (see Fig. 1).

Taking into account the beneficial influence of vacuum mentioned in Section 1, we could obtain a junction of a good quality with the following set of parameters: vacuum 10^{-5} mbar, temperature 1100 °C, contact pressure 9 MPa, annealing duration 60 h. In addition, a series of experiments with different values of pressure and time were carried out.

After each experiment, we could estimate the bonded area in the interface from optical examination of the interface through the α-Al_2O_3 platelet. This observation could even be made easier by using a coloured penetrating spray generally available for microcrack detection.

The detailed procedure for the preparation of cross-sectional specimens for transmission electron microscopy (TEM) has been presented elsewhere [32]. Its main difficulty lay in the marked brittleness of the foils, and their propensity to self-destruction by adhesive interfacial rupture after a few hours of observation time. This was attributed to the probably high level of residual thermal stresses remaining in these massive two-phase specimens after cooling from the annealing temperature. However, it was possible to carry out a sufficient number of concluding preliminary observations which will be presented below.

4. Results and discussion

4.1. Influence of annealing conditions on the solid-state bonding kinetics

We chose the bonded fraction R of the contact area to characterize the extent of the junction obtained for a given set of bonding-treatment parameters which we were able to change: annealing time and external applied pressure normal to the contact surfaces, with fixed temperature and vacuum (1100 °C, 10^{-5} mbar). R is defined as the ratio

$$R = \text{bonded area/total contact area} \quad (6)$$

This parameter can be experimentally measured and is also direct result of calculations carried out according to Garmong *et al.*'s model [25].

Fig. 2 presents the calculated results compared to the experimental ones. As expected, the bonded fraction increases with time and applied pressure, and both calculations and experiments confirm these logical tendencies. As in previous works on metal couples [27, 28], it can be seen both from calculations and experiments that the applied pressure seems to be more efficient than time to accelerate the bonding process. However, when dealing with oriented single crystals, the bonding pressure may not be increased freely because of possible recrystallization. In the present case, we took care to operate far enough from the recrystallization region, which may be situated between 20 and 200 MPa at 1100 °C according to a deformation mechanism map due to Ashby, as reported by Gittus [29]. Temperature, the influence of which was not studied in the present work, is probably still more efficient than pressure to ensure a rapid bonding: indeed, for instance, Drillet reported a successful bonding after only 30 min at 1400 °C, 2 MPa, under vacuum [1]. However, it can be verified in our case that the set of conditions resumed as 10^{-5} mbar, 1100 °C, 9 MPa, 60 h, was correctly chosen to provide a complete bonding.

It may also be noticed in Fig. 2 that, except for $R = 1$, the experimental values of R systematically ex-

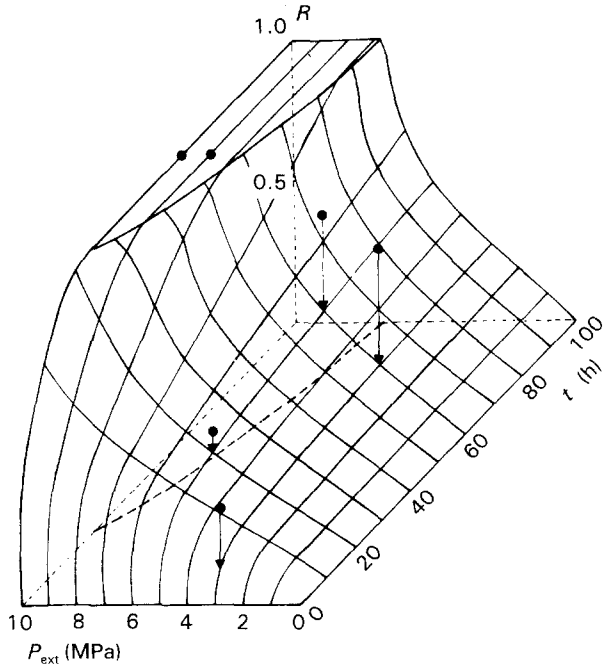

Figure 2 Variations of the bonded fraction, R, of the contact area versus the applied pressure and the annealing time at the welding temperature (1100 °C) (R = bonded area/total contact area). (——) Calculations according to Garmong *et al.*'s model [25]. (●) Experimental measurements on the specimens.

ceed the calculated ones. Indeed, the estimated bonded area is probably always superior to the real value, because some small-size closed interfacial cavities must remain undetected at optical examination. In addition, uncertainties in the data (such as γ, D_v and the constants in creep law) taken for the calculation following Equations 3 and 4 may possibly produce a systematic under-estimation of the theoretical value of R.

Nevertheless, the order of magnitude of the experimental time and pressure leading to $R = 1$ seems to be correctly predicted by the present model.

4.2. Solid-state bonding models

Other models have been proposed to describe the kinetics of achievement of the full physical contact along the interface between a metal and a ceramic obtained by solid-state bonding, especially by Klomp. In his first model [2], two mechanisms are taken into account: evaporation–condensation of the metal, and diffusion of vacancies. The porosities left in the interface after contact are partly filled by a metallic layer evaporated from the metal surface and condensed on the ceramic surface. As far as the volume of the pore is concerned, this evaporated layer has no effect in our opinion, because the material involved comes from the opposite face of the pore. The only interest of this condensed metal layer, from the point of view of kinetics, is to change the shape of the cavity and to increase the extension of the metallic surface on which an active surface diffusion is enhanced: the triple lines could thus reach an equilibrium configuration more rapidly, together with the replacement of the interface between ceramic and metallic vapour by a ceramic/solid metal interface.

According to Klomp [2], the time for a condensed metal monolayer to be obtained is given by

$$t = \frac{da}{W} \tag{7}$$

where a is the crystal lattice parameter of the metal, d the metal density, and W the metal vapour flux per cm^2 and per second

$$W = c\frac{P_s M^{1/2}}{T^{1/2}} \tag{8}$$

where P_s is the saturated vapour pressure of the metal with atomic mass M at absolute temperature T. An example was given by Klomp for iron at 1648 K, where $t = 2 \times 10^{-2}$ s. Assuming that the constant factor, c, for nickel is of the same order as for iron, and taking the value of saturated pressure $P_s = 3 \times 10^{-6}$ mbar [33], it can be deduced in our case that $t \approx 20$ s, at 1373 K.

The second mechanism associated by Klomp [2] with the previous one is the vacancy diffusion from the porosity towards the solid. The equation that describes the kinetics of volume reduction is written as

$$-\frac{dV}{dt} = \frac{8\pi D_s \gamma_m \Omega}{kT} \tag{9}$$

where V is the pore volume, t the time, D_s the self-diffusion coefficient, Ω the vacancy volume, γ_m the surface energy of the metal, k Boltzmann's constant, and T the absolute temperature. D_s is given by

$$D_s = D_0 \exp\left(-\frac{Q_s}{RT}\right) \tag{10}$$

where Q_s is the activation energy for self-diffusion, and R is the universal gas constant.

It should be noted that Equation 9 is similar to one of the kinetics terms taken into account by Garmong *et al.* [25] for Stage II (see Equation 4). For the couple Al_2O_3/Ni with the same data as in Table IV it is found that

$$-dV/dt = 2.754 \times 10^{-10}\ mm^3 h^{-1} \tag{11}$$

So it requires $t = 1.9$ h to close a 1 μm diameter pore, whatever the applied pressure, because the model neglects the effect of this parameter, which is obviously unrealistic.

In his second model [3], Klomp neglects the effect of evaporation–condensation, keeps the effect of vacancy diffusion described by Equation 9, and adds a contribution of the plasticity of the metal phase, which allows the introduction of the applied pressure through the relation

$$A = F/R_e \tag{12}$$

where A is the real contact area between the solid surfaces, F the applied load perpendicular to the interface, and R_e the yield stress of the metal at the welding temperature. Joining Garmong *et al.*'s arguments [25], this plasticity allows a fast achievement of the physical contact on an increasing extent and from

there onwards, the remaining pores are closed with help of vacancy diffusion.

Both of these models give rather unrealistic predictions with regards to our experimental results. Comparing them to the model we used, it seems to us that their physical bases are similar and that Garmong's model is actually more sophisticated than Klomp's second scheme, and thus more likely to describe the reality. Consequently, and as confirmed by experimental facts, we rather rely on Garmong *et al.*'s model [25] to predict Al_2O_3/Ni solid-state bonding kinetics. The micrograph in Fig 3, taken in the scanning electron microscope (SEM) on a solid-state bonded interface between nickel and a polycrystalline alumina slice with important surface roughness, provides experimental support to our assumption of undeformability of the ceramic. It can be seen that the alumina remained undeformed and that nickel has filled up the superficial asperities by plastic deformation and vacancy diffusion. It may be argued that the need for the metal alone to fill the surface asperities without the help of any ceramic creep will change the kinetical and geometrical conditions from those originally assumed by Garmong *et al.* [25]. In fact, Equation 3 for Stage I is insensitive to the depth of the long-range asperities, and only depends on the dimensionless width, u, of the transverse slices of creeping material. The decisive effect for the duration of Stage I is the lateral extension of the slices rather than their thickness reduction, until the remaining cavity has a size comparable with the short wavelength asperities. This is not affected by the fact that both or only one material creeps, especially with the slightly convex geometry of the contact faces of our specimens. During Stage II, only the metal will contribute to the final closure of the voids. This is what we assumed by taking data for nickel only to solve Equation 4, and neglecting creep, vacancy diffusion and surface-energy driving force on the ceramic side. This is also supported by the fact that the evaporation–condensation process will produce a metal coating inside the pore in a very short time, as calculated above. Actually, even integrating Equation 4 for a double initial value of the cavity size to account for the rigidity of the ceramic, gives less than twice the closure time, which is in any case much shorter than the duration of Stage I.

One main limitation to this solid-state bonding model is, however, that it does not take into account any chemical reaction between the contacting materials. The kinetics and mechanism of formation, diffusion characteristics, and mechanical behaviour of the reaction product would have to be included for interfaces between reacting materials. Apart from this case, it may be anticipated that its application would be equally successful to other ceramic–metal non-reacting couples within the framework of the same hypotheses we assumed.

4.3. Al_2O_3/Ni interface observation

Optical microscopy and scanning electron microscopy on cross-sections of the bonded specimens did not reveal more than a planar phase boundary. Concentration profiles across the interphase were recorded on an electron microprobe. No concentration gradient nor intermediate layer could be detected at that scale of measurement.

Transmission electron microscopy was performed with a Jeol 200 CX microscope operated at 200 keV. The first verification we made on our foils concerned the relative orientations of the two crystals at the interface. The TEM diffraction patterns in Fig. 4

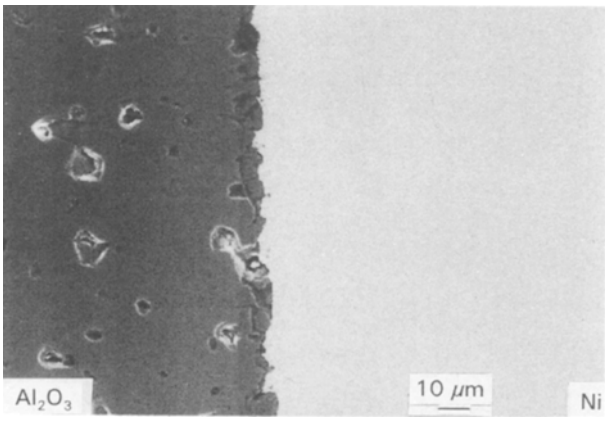

Figure 3 SEM image of an interface Ni/Al_2O_3 (polycrystal) obtained at 9 MPa, 1100 °C, 10^{-5} mbar, 60 h. Notice the undeformed asperities of alumina.

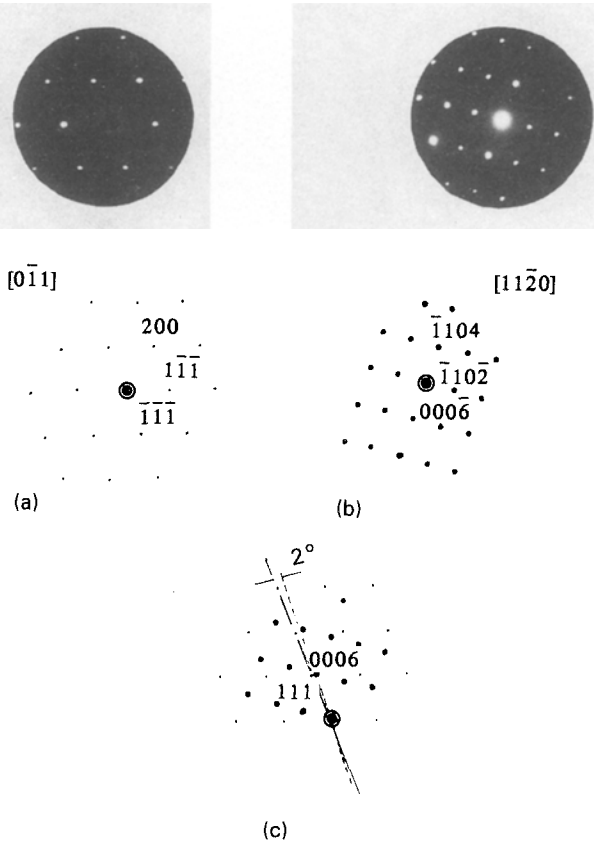

Figure 4 (a, b) TEM diffraction patterns (200 kV, $e^- \| [0\bar{1}1]_{Ni} \| [11\bar{2}0]_{Al_2O_3}$), respectively, on the nickel and Al_2O_3 side of a diffusion-bonded interface. (c) Superimposition of the diagrams shows the persistence of the initially fixed orientation relationships within $\pm 2°$

illustrate the results of these observations on a foil with the interface plane normal to the foil plane and parallel to the electron beam. It may be seen that:

(i) the relative orientations deduced from the obtained diagrams for a position of the foil with a zero tilt angle are consistent with those chosen for bonding (see Fig. 1);

(ii) superimposing the two diagrams shows a coincidence of the normals to planes $(0\,0\,0\,1)_{Al_2O_3}$ and $(1\,1\,1)_{Ni}$ with a 2° discrepancy, which stays within the limits of the experimental uncertainty on the Läue patterns and positioning of the specimens.

Fig. 5 shows an example of observations carried out in a transparent zone containing the interface normal to the picture. The micro-relief visible on the surfaces of the foil is probably due to the final ion-thinning operation. It is verified with the help of the diffraction diagram of alumina that the diffraction vector **g** $(0\,0\,0\,6)_{Al_2O_3}$ is approximately (± 5°) perpendicular to the interface plane, after correction for image/diagram rotation. The phase boundary appears to be flat and free from any reaction layer at this scale of observation. So we can confirm that it is possible to obtain Al_2O_3/Ni interfaces free from spinel compound by performing the thermocompression annealing under vacuum, and starting with sufficiently oxygen-free materials [1, 12]. In their work, Trumble and Rühle [12] suggest that the formation of spinel requires a

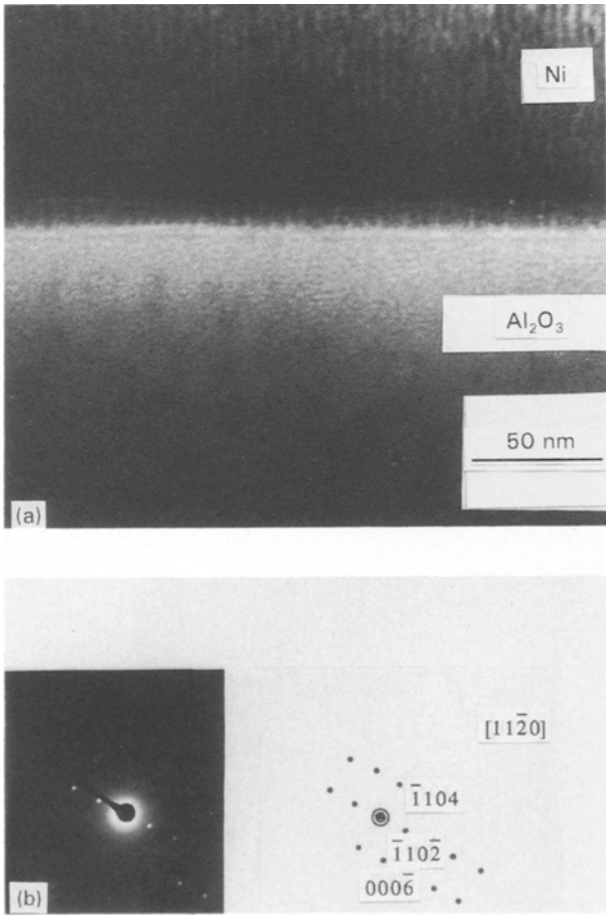

Figure 5 Interface of a bicrystal Ni/Al_2O_3 (TEM, 200 kV, $e^- \| [0\,\bar{1}\,1]_{Ni} \| [1\,1\,\bar{2}\,0]_{Al_2O_3}$). (a) bright field, $g = (0\,2\,\bar{2})_{Ni}$; (b) diffraction patterns in alumina.

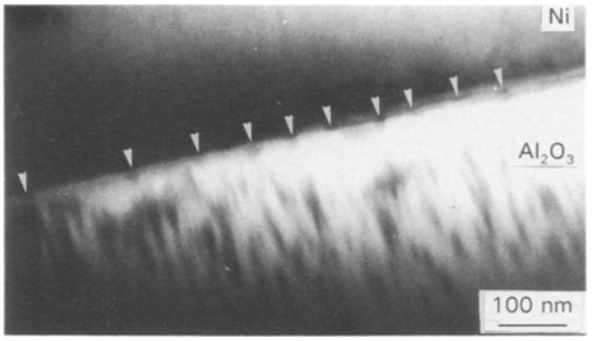

Figure 6 "Fish bone" contrasts in Al_2O_3 (TEM, 200 kV, bright-field, $g = \{1\,1\,3\}_{Ni}$). Also note the quasi-periodic dark contrasts along the interface (arrows).

minimum oxygen concentration at the interface during annealing, which they estimate to be about 100 at. p.p.m. at 1100 °C from thermodynamical arguments. When the bonding is conducted under clean vacuum, the main possible source for oxygen is then the nickel impurity, which was checked to be less than 49 at. p.p.m. in our case as mentioned earlier. However, by high-resolution TEM, Drillet [1] could see a 2 nm layer of nickel oxide, NiO, which we have not been able to detect so far on our specimens. In the thickest parts of the foil, peculiar contrasts may be seen on the alumina side (Fig. 6), forming slender tips perpendicular to the interface. This type of contrast had also been observed by Drillet [1] who termed them "fish bone" images. They were attributed either to an artefact of ion thinning (redeposition) or more likely to an effect of residual stresses. We noticed that these features are only visible in the thickest regions of the foil, which explains the poor quality of our micrograph. On the same picture, reinforcements of the contrast are detectable in the interface at the base of the slender tips. These dark spots with an average distance of about 50 nm resemble some periodic interfacial contrasts observed by Mader and Rühle [34] and attributed by the authors to the strains associated with interface facets. These contrasts also disappear in the thinner zones of the foil. It is considered that a more specific investigation will be needed to elucidate the origin of the contrasts.

Acknowledgement

The authors thank Doctor R. Bonnet for access to the CSL computer programs and helpful advice on their use.

References

1. P. DRILLET, Doctorate Thesis, University of Rennes, France (1991).
2. J. T. KLOMP, *Sci. Ceram.* **5** (1970) 501.
3. J. T. KLOMP, *Proc. Br. Ceram. Soc.* **34** (1984) 249.
4. C. A. CALOW, R. D. BAYER and I. T. PORTER, *J. Mater. Sci.* **6** (1971) 150.
5. C. A. CALOW and I. T. PORTER, *ibid.* **6** (1971) 156.
6. H. J. de BRUIN, A. F. MOODIE and C. E. WARBLE, *ibid.* **7** (1972) 909.

7. M. NICHOLAS and D. A. MORTIMER, in Proceedings of Young Metallurgists Spring Meeting, Palma, Majorca, March 1974, "Practical Metallic Composites" (Institution of Metallurgists, London, 1974) p. C 27.
8. F. P. BAILEY and W. E. BORBIGE, in "Surface and Interface in Ceramics and Ceramic-Metal Systems", edited by J. Pask and A. Evans, Materials Science Research, Vol. 14 (Plenum Press, New York, London, 1981) p. 525.
9. M. G. GEE, *Proc. Brit. Ceram. Soc.* **34** (1984) 261.
10. M. G. NICHOLAS, *Braz. Solder.* **10** (Spring) (1986) 11.
11. J. A. WASYNCZUK and M. RÜHLE, in Proceedings of "Ceramic Microstructures' 86, Role of Interfaces", edited by J. A. Pask and A. G. Evans, Materials Science Research, Vol. 21 (Plenum Press, New York, London, 1987) p. 341.
12. K. P. TRUMBLE and M. RÜHLE, *Mater. Res. Soc. Symp. Proc.* **138** (1989) 551.
13. G. HASSON, J. Y. BOOS, I. HERBEUVAL, M. BISCONDI and C. GOUX, *Surf. Sci.* **31** (1972) 115.
14. A. P. SUTTON, in Proceedings "I.I.B.-89", Paris, 4–8 Sept. 1989 (Editions de Physique, Paris, 1990). Colloque C1, no. 1, Vol. 51 (1990) p. 35.
15. W. BOLLMANN, in "Crystal Defects and Crystalline Interfaces" Edited by W. Bollman (Springer, Berlin, 1970).
16. *Idem, Philos. Mag.* **16** (1970) 363.
17. *Idem, ibid.* **16** (1970) 384.
18. R. BONNET and F. DURAND, *ibid.* **32** (1975) 997.
19. R. BONNET and E. COUSINEAU, *Acta Crystallogr.* **A33** (1977) 850.
20. R. BONNET, *Mater. Res. Soc. Symp. Proc.* **122** (1988) 282.
21. C. A. M. MULDER and J. T. KLOMP, *J. Phys. Coll. C4* Suppl. no. 4, **46** (1985) 111.
22. H. F. FISCHMEISTER, W. MADER, B. GIBBESCH and G. ELSSNER, *Mater. Res. Soc. Symp. Proc.* **122** (1988) 529.
23. A. CATANA, P. E. SCHMID, M. HEINTZE, F. LEVY, P. STADELMANN and R. BONNET, *J. Appl. Phys.* **67** (1990) 1820.
24. P. ALDEBERT and J. P. TRAVERSE, *J. Am. Ceram. Soc.* **65** (1982) 460.
25. G. GARMONG, N. E. PATON and A. S. ARGON, *Met. Trans.* **6A** (1975) 1269.
26. C. H. HAMILTON, in "Proceedings of the Second International Conference on Titanium Science and Technology", Vol. 1, edited by R. I. Jaffee and H. M. Burte (Plenum Press, New York, 1973) p. 625.
27. M. DUPEUX, *J. Cryst. Growth* **66** (1984) 169.
28. M. DUPEUX, H. ROUAULT-ROGEZ and P. WILLEMIN, *Mater. Res. Soc. Symp. Proc.* **122** (1988) 169.
29. J. GITTUS, "Creep, Viscoelasticity and Creep Fracture in Solids" (Applied Science London, 1975).
30. N. EUSTATHOPOULOS, J. C. JOUD and P. DESRE, *J. Chim. Phys.* **1** (1973) 42.
31. H. ROUAULT-ROGEZ, Doctorate Thesis, Institut National Polytechnique of Grenoble, France (1990).
32. C. WAN and M. DUPEUX, *J. Electron Microsc. Techn.* **23**(3) (1992) 248.
33. J. LAPUJOULADE, *Le Vide* **95** (1961) 207.
34. W. MADER and M. RÜHLE, *Acta Metall.* **37** (1989) 853.

Received 10 March 1992
and accepted 15 January 1993